THE JOURNAL OF PHYSICAL CHEMISTRY A LETTERS

2007, *111,* 1163−1166
Published on Web 01/12/2007

Frequency- and Time-Resolved Coherence Transfer Spectroscopy

Mark A. Rickard, Andrei V. Pakoulev, Nathan A. Mathew, Kathryn M. Kornau, and John C. Wright*

Department of Chemistry, University of Wisconsin, Madison, Wisconsin 53706

Received: November 22, 2006

Frequency-domain two-color triply vibrational enhanced four-wave mixing using a new phase-matching geometry discriminates against coherent multidimensional spectral features created solely by radiative transitions, spectrally resolves pathways with different numbers of coherence transfer steps, and temporally resolves modulations created by interference between coherence transfer pathways. Coherence transfer is a nonradiative transition where a superposition of quantum states evolves to a different superposition. The asymmetric and symmetric C≡O stretching modes of rhodium(I) dicarbonyl acetylacetonate are used as a model system for coherence transfer. A simplified theoretical model based on Redfield theory is used to describe the experimental results.

Coherent multidimensional four-wave mixing (FWM) involves three radiative transitions that excite a series of vibrational or electronic coherences (entangled quantum states), and the last coherence emits the output signal.[1−3] Multiple pathways that create the same output coherence interfere at the amplitude level. Nonradiative coherence transfer (CT) can change the pathways and create additional weak spectral features.[4,5] Since coherence transfer identifies coupled quantum states, it potentially can form the basis for new methods of coherent multidimensional spectroscopy.

Time-domain two-dimensional infrared (2D-IR) spectroscopy uses femtosecond lasers to excite all the quantum states within the excitation bandwidth.[6−8] Typically, one measures the temporal phases of the first and last coherences of each pathway, and a 2D Fourier transform creates a 2D spectrum with cross-peaks that reveal correlations between quantum states created by inter- and intramolecular interactions. The intermediate coherences (or populations) created after the second excitation are not usually measured. Coherence transfer increases the possible pathways and the complexity of the 2D-IR spectra.[4]

Quantum mechanically, coherence transfer is an amplitude-level process mediated by the thermal environment in which an initial superposition of states evolves to a different superposition. Some coherence transfer pathways create new peaks in 2D-IR spectra, but most overlap stronger peaks that only involve radiative transitions. Implementation of coherence transfer multidimensional spectroscopy requires discrimination between the strong radiative pathways and the weaker coherence transfer pathways.

Frequency-domain FWM spectroscopies excite one specific quantum state with each excitation pulse. This specificity discriminates between coherence transfer and purely radiative pathways. Coherence transfer pathways involve coherences that could not be created by radiative transitions so the coherence transfer pathways are spectrally resolved. Triply vibrationally enhanced (TRIVE) FWM experiments[9−12] demonstrated that spectrally resolving the coherence transfer pathways created interferometric temporal modulations because of quantum-level interference between equivalent pathways.[13] In this Letter, we show that adopting a different phase-matching geometry strongly discriminates against purely radiative pathways, isolates the coherence transfer pathways, and forms the basis for coherence transfer spectroscopy where cross-peaks between quantum states are generated by nonradiative transfer between molecular coherences.

The experiment uses a mode-locked Ti:sapphire oscillator/regenerative amplifier to pump two independently tunable optical parametric amplifiers that create mid-infrared laser pulses (pulse width of 900 fs, bandwidth of 20 cm^{-1}, frequencies of ω_1 and ω_2). The ω_2 beam is split to create a third beam, designated $\omega_{2'}$, and all beams are identically polarized. The beams are focused into the sample with an off-axis parabolic mirror at angles defined by phase matching, $\vec{k}_{CT} = -\vec{k}_1 + \vec{k}_2 + \vec{k}_{2'}$ (subscripts designate frequency, not time ordering). Previous work used $\vec{k}_N = \vec{k}_1 - \vec{k}_2 + \vec{k}_{2'}$.[13] The signal is spectrally resolved with a monochromator (ω_m) and MCT detector. The output intensity is recorded as a function of ω_1, ω_2, ω_m, $\tau_{2'1}$, and τ_{21} where the time delay (τ_{ij}) is defined as $\tau_{ij} \equiv \tau_i - \tau_j$ and τ_i corresponds to the temporal position of the k_i beam. Scans of $\tau_{2'1}$ and τ_{21} with fixed ω_1, ω_2, and ω_m measure the dynamics for all FWM time-ordered pathways. Table 1 defines the time-ordered pathways labeled I−VI.[9,10]

The sample is a 200 μm thick solution of ≈1.5 mM rhodium(I) dicarbonyl acetylacetonate, $Rh(CO)_2acac$, in hexane. $Rh(CO)_2acac$ has an asymmetric CO stretch (labeled *a*) at 2015 cm^{-1} and a symmetric CO stretch (labeled *s*) at 2084 cm^{-1} relative to the ground state (labeled *g*). The vibrational modes have anharmonicities of 14, 11, and 26 cm^{-1} for the asymmetric stretch overtone (2*a*), the symmetric stretch overtone (2*s*), and their combination band (*a*+*s*), respectively.[4] This paper focuses

* To whom correspondence should be addressed. E-mail: wright@chem.wisc.edu.

10.1021/jp0677804 CCC: $37.00

TABLE 1: Time-Ordered TRIVE FWM Pathways

time ordering					
I	II	III	IV	V	VI
$\tau_{2'1} > \tau_{21} > 0$	$\tau_{21} > \tau_{2'1} > 0$	$\tau_{2'1} > 0; \tau_{21} < 0$	$\tau_{2'1} < 0; \tau_{21} > 0$	$\tau_{21} < \tau_{2'1} < 0$	$\tau_{2'1} < \tau_{21} < 0$

on the cross-peak between the symmetric and asymmetric stretches at $(\omega_1, \omega_2) = (2084, 2015)$ cm^{-1}.

Earlier work observed CT using the phase-matching condition $\vec{k}_N = \vec{k}_1 - \vec{k}_2 + \vec{k}_{2'}$. The following coherence pathways (time ordering of $-k_2$, k_1, and $k_{2'}$) are representative examples of the $\vec{k}_N$ geometry with zero, one, or two coherence transfers, respectively:

$$g, g \xrightarrow{-2} g, a \xrightarrow{1} s, a \xrightarrow{2'} s, g \quad \text{(A)}$$

$$g, g \xrightarrow{-2} g, a \overset{\text{CT}}{\Longrightarrow} g, s \xrightarrow{1} g, g \xrightarrow{2'} a, g \quad \text{(B)}$$

$$g, g \xrightarrow{-2} g, a \overset{\text{CT}}{\Longrightarrow} g, s \xrightarrow{1} g, g \xrightarrow{2'} a, g \overset{\text{CT}}{\Longrightarrow} s, g \quad \text{(C)}$$

The indices (i, j) designate the $\rho_{i,j}$ coherence formed after each interaction that has a frequency of $\omega_{i,j} \equiv \omega_i - \omega_j$. Single arrows indicate radiative transitions, and double arrows indicate coherence transfer. In all cases, transitions induced by ω_1 and ω_2 involve resonances with modes s and a, respectively.

All of the coherences in pathway A are created by radiative transitions. Pathways B and C involve one or two CT events, respectively. The output at $\omega_{s,g}$ from pathways A and C is identical in frequency and direction, so it is not possible to observe pathway C by itself; it is hidden by the dominant contribution from A. Pathway B (output at $\omega_{a,g}$) is spectrally resolved from A and C (output at $\omega_{s,g}$) and may be distinguished from the much larger intensity of pathway A.

The $\vec{k}_{\text{CT}} = -\vec{k}_1 + \vec{k}_2 + \vec{k}_{2'}$ phase-matching condition suppresses pathways without coherence transfer and spectrally resolves one- and two-CT processes. The following coherence pathways with zero, one, or two coherence transfers, respectively, and time ordering III (k_2, $-k_1$, and $k_{2'}$) illustrate these characteristics:

$$g, g \xrightarrow{2} a, g \xrightarrow{-1} a, s \xrightarrow{2'} 2a, s \quad \text{(D)}$$

$$g, g \xrightarrow{2} a, g \overset{\text{CT}}{\Longrightarrow} s, g \xrightarrow{-1} g, g \xrightarrow{2'} a, g \quad \text{(E)}$$

$$g, g \xrightarrow{2} a, g \overset{\text{CT}}{\Longrightarrow} s, g \xrightarrow{-1} g, g \xrightarrow{2'} a, g \overset{\text{CT}}{\Longrightarrow} s, g \quad \text{(F)}$$

The output signal from pathway D requires a "forbidden" three-quantum transition, where two quanta of state a are destroyed and one quantum of state s is created in the transition. Consequently, this pathway, which does not involve CT, is much weaker than the corresponding pathway A in the $\vec{k}_N$ geometry. Furthermore, pathways D, E, and F have different emission frequencies of $\omega_{2a,s}$, $\omega_{a,g}$, and $\omega_{s,g}$, respectively, that can be spectrally resolved. In summary, the $\vec{k}_{\text{CT}}$ geometry allows direct observation of all CT pathways without interference from purely radiative pathways.

Figure 1 shows the relevant Liouville diagrams for time orderings I/II and III/IV with frequencies of $(\omega_1, \omega_2) = (\omega_{s,g}, \omega_{a,g}) = (2084, 2015)$ cm^{-1}. Pathways with one transfer have output frequencies of $\omega_{a,g} = 2015$ cm^{-1}, $\omega_{2a,a} = 2001$ cm^{-1}, and $\omega_{a+s,s} = 1989$ cm^{-1}. Two transfers lead to $\omega_{s,g} = 2084$ cm^{-1}, $\omega_{2s,s} = 2073$ cm^{-1}, and $\omega_{a+s,a} = 2058$ cm^{-1} output frequencies for this set of ω_1 and ω_2 frequencies. The purely radiative pathway's signal occurs at $\omega_{2a,s} = 1932$ cm^{-1}.

A one-dimensional scan of FWM intensity versus monochromator frequency with fixed laser frequencies of $(\omega_1, \omega_2) = (2084, 2015)$ cm^{-1} and time delays of $(\tau_{2'1}, \tau_{21}) = (0.0, 0.0)$ ps appears in Figure 2a. The spectrum clearly shows three output transitions at 1932, 1988, and 2015 cm^{-1} that are created by the $(2a, s)$, $(a+s, s)$, and (a, g) coherences, respectively. The peaks at 1988 and 2015 cm^{-1} require one CT (see Figure 1). Further confirmation that these peaks are created by coherence transfer is shown in Figure 2b, which is a contour plot of FWM intensity versus τ_{21} and ω_{m} at $\tau_{2'1} = -0.3$ ps. Cross sections of the data at monochromator frequencies of 2015, 1988, and 1932 cm^{-1} are shown above the contour plot. The peak at 1932 cm^{-1} relaxes exponentially without modulation, as expected for a pathway that does not involve CT. The peak at 2015 cm^{-1} is modulated with a period of 480 fs (frequency of 69 cm^{-1}), and the peak at 1988 cm^{-1} has two components with periods of 480 and 800 fs (frequencies of 69 and 42 cm^{-1}, respectively). It is important to note that the modulation time scale is much faster than the 900 fs pulse width of the laser. There is no evidence of peaks at $\omega_{s,g}$, $\omega_{2s,s}$, and $\omega_{a+s,a}$ in Figure 2a that would indicate the presence of pathways requiring two coherence transfers.

The quantum beating present at 1988 and 2015 cm^{-1} is characteristic of coherence transfer. Using the approach described in previous work,[13,14] the ket-side coherence transfer $a, g \xrightarrow{\text{CT}} s, g$ has the following forms for the initial coherence (eq 1) and final coherence (eq 2):

$$\rho_{a,g}(t) \approx \mathrm{e}^{(-i\omega_{a,g} - \Gamma_{a,g})t} \quad (1)$$

$$\rho_{s,g}(t) \approx \frac{\kappa_{a,g;s,g}}{i(\omega_{s,g} - \omega_{a,g}) + \Gamma_{s,g} - \Gamma_{a,g}} \times [\mathrm{e}^{(-i\omega_{a,g} - \Gamma_{a,g})t} - \mathrm{e}^{(-i\omega_{s,g} - \Gamma_{s,g})t}] \quad (2)$$

where $\kappa_{a,g;s,g}$ is the transfer rate from (a, g) to (s, g) and $\Gamma_{i,j}$ is the dephasing rate of coherence (i, j). Equation 2 has the opposite sign for a bra-side coherence transfer. Equation 2 reveals that any coherence created by CT oscillates at two frequencies, the frequency of the initial coherence and the frequency of the final coherence. Consequently, the FWM intensity, $I(t) \propto |\rho(t)|^2$, beats at the difference frequency of these two coherences as they evolve in time. Additionally, interference between all equivalent pathways in Figure 1 must be included to describe the observed $\tau_{2'1}$, τ_{21} dependence.

For values of $\tau_{21} > 0$ ps in Figure 2b, time orderings II and IV are relevant, and varying τ_{21} probes the coherence created after the second laser interaction, which in this case is formed by coherence transfer from (a, s) to (a, a). For values of $\tau_{21} < 0$ ps, time ordering III is relevant, and varying τ_{21} probes the coherence created after the first laser interaction, which in this case is formed by coherence transfer from (a, g) to (s, g). In both cases, the difference frequency is 69 cm^{-1} and accounts for the beating in Figure 2b. The 42 cm^{-1} frequency in the 1988 cm^{-1} peak cannot be attributed to coherence transfer in four-wave mixing. It is created by coherence transfer in six-wave mixing and will be explained fully in a later publication.

The temporal dependence of coherence transfer can be used to determine the relative importance of each transfer pathway. Figure 3a shows the $\tau_{2'1}$, τ_{21} dependence for the coherence

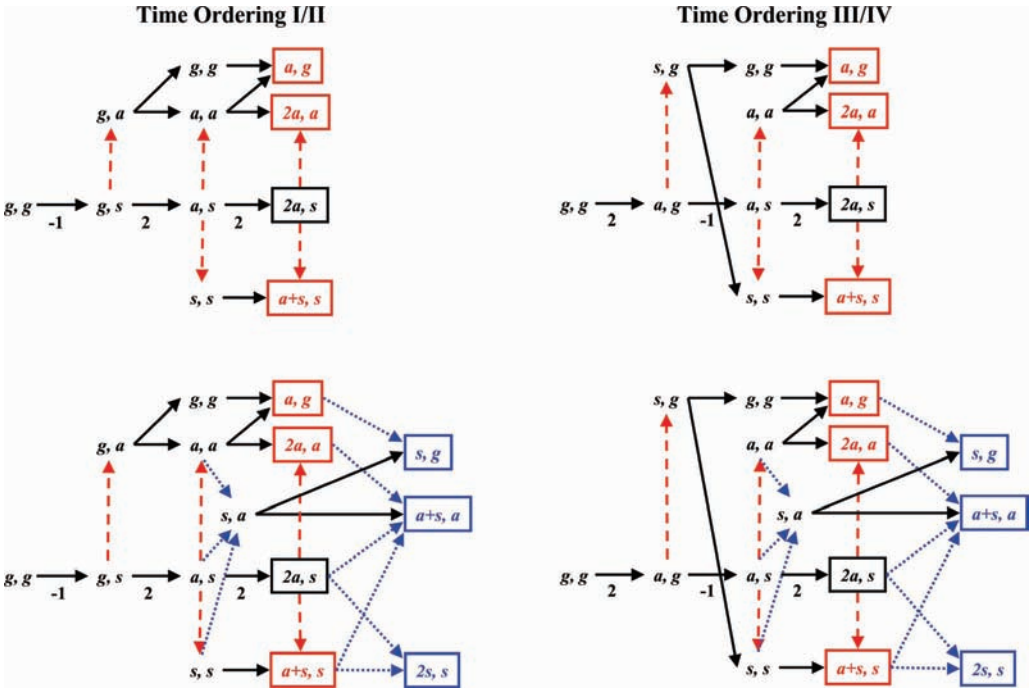

Figure 1. Liouville diagrams that describe the flow of coherences from the initial ground state population (g, g) to the final radiating coherence for frequencies (ω_1, ω_2) = ($\omega_{s,g}$, $\omega_{a,g}$). Laser interactions with ω_2 and $\omega_{2'}$ are equivalent in these diagrams, and the notation has been simplified to ω_2. Black solid arrows represent radiative transitions, red dashed arrows are the first CT, and blue dotted arrows are the second CT. Interactions like $a, s \xrightarrow{CT} s, a$ or $2a, s \xrightarrow{CT} 2s, s$ that change two quanta in a single step are indicated in blue as the second CT. Final radiating coherences are enclosed in boxes and colored black, red, and blue for pathways with zero, one, and two transfers, respectively. Time ordering V/VI was omitted because it does not contribute significantly to the observed CT pathways.

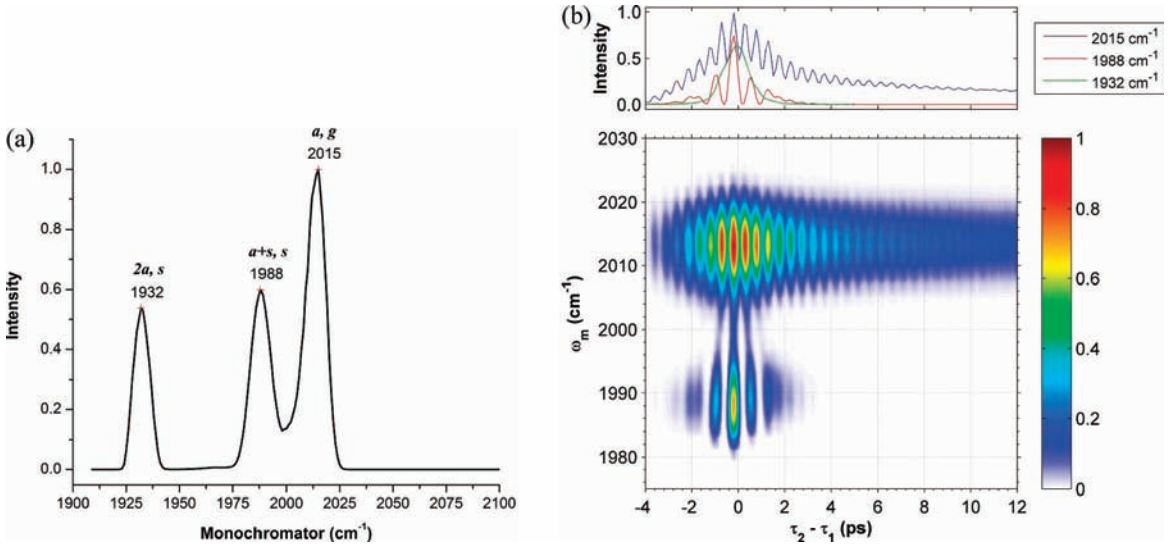

Figure 2. (a) One-dimensional scan of FWM intensity versus monochromator frequency with fixed laser frequencies (ω_1, ω_2) = (2084, 2015) cm^{-1} and time delays ($\tau_{2'1}$, τ_{21}) = (0.0, 0.0) ps. (b) Contour plot of FWM intensity versus τ_{21} and ω_m at (ω_1, ω_2) = (2084, 2015) cm^{-1} and $\tau_{2'1}$ = −0.3 ps. Cross sections of the data at ω_m = 2015, 1988, and 1932 cm^{-1} are shown above the contour plot.

transfer peak at (ω_1, ω_2, ω_m) = (2084, 2015, 2015) cm^{-1}. The quantum beats have a period of 480 fs in both temporal dimensions. This dependence contrasts with experimental results in previous work which had modulations only in τ_{21}.[13] The data is symmetric about the $\tau_{21} = \tau_{2'1}$ axis because interactions with ω_2 and $\omega_{2'}$ are equivalent with the k_{CT} phase-matching condition.

The only pathways required to explain the τ_{21}, $\tau_{2'1}$ dependence in Figure 3 are those with one coherence transfer that create an $\omega_{a,g}$ signal. The complete temporal dependence of time ordering III is described as an example. For time ordering III (k_2, $-k_1$, and $k_{2'}$), there are two pathways ($a, g \xrightarrow{CT} s, g$ and $a, s \xrightarrow{CT} a, a$) that contribute to quantum beating (eq 3).

$$\rho_{a,g}(t) = \frac{\kappa_{a,g;s,g}}{i(\omega_{s,g} - \omega_{a,g}) + \Gamma_{s,g} - \Gamma_{a,g}}[(e^{(-i\omega_{a,g}-\Gamma_{a,g})\tau_{12}} - e^{(-i\omega_{s,g}-\Gamma_{s,g})\tau_{12}})e^{-\Gamma_{gg}\tau_{2'1}}e^{(-i\omega_{a,g}-\Gamma_{a,g})(t-\tau_{2'})}] - \frac{\kappa_{a,s;a,a}}{i(0 - \omega_{a,s}) + \Gamma_{a,a} - \Gamma_{a,s}}[e^{(-i\omega_{a,g}-\Gamma_{a,g})\tau_{12}}(e^{(-i\omega_{a,s}-\Gamma_{a,s})\tau_{2'1}} - e^{-\Gamma_{a,a}\tau_{2'1}})e^{(-i\omega_{a,g}-\Gamma_{a,g})(t-\tau_{2'})}] \quad (3)$$

This treatment assumes the impulsive, weak field, and Bloch limits and neglects population transfer. On the basis of the pulse ordering, the natural time delays for these pathways are $\tau_{12} \equiv$

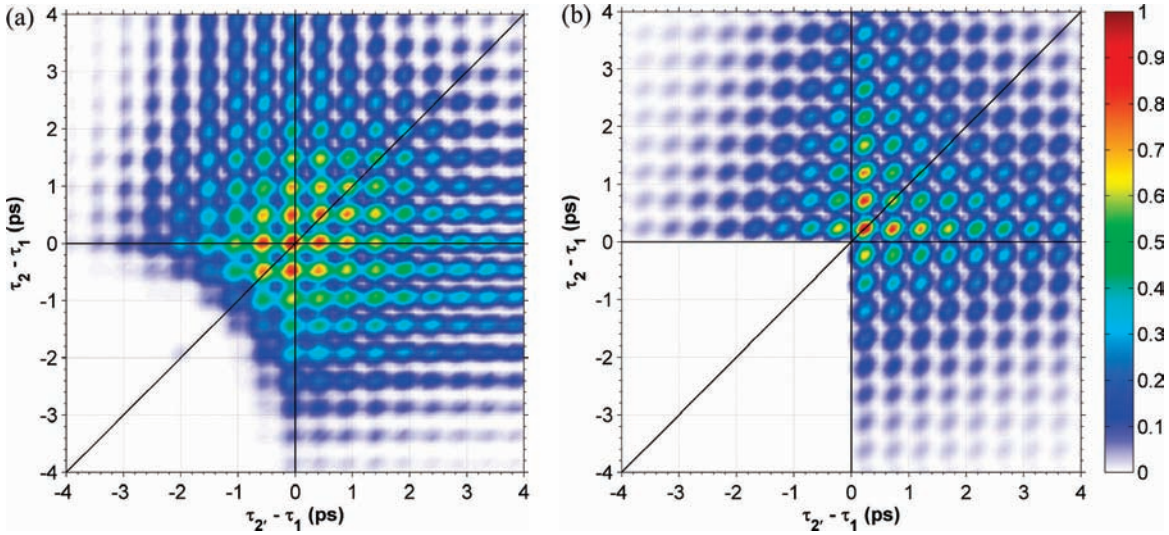

Figure 3. (a) Contour plot of FWM intensity versus $\tau_{2'1}$ and τ_{21} for the coherence transfer peak at (ω_1, ω_2, ω_m) = (2084, 2015, 2015) cm^{-1}. (b) Theoretical simulation of part a using the parameters $\kappa_{g,s;g,a} = \kappa_{a,s;a,a}$, $\kappa_{a,g;s,g} = 0.72\kappa_{g,s;g,a}$, $1/\Gamma_{a,g} = 3.0$ ps, $1/\Gamma_{s,g} = 3.5$ ps, $1/\Gamma_{a,s} = 3.4$ ps, $1/\Gamma_{g,g} =$ 40 ps, and $1/\Gamma_{a,a} = 3.8$ ps.

$-\tau_{21}$ and $\tau_{2'1}$. The origins of the beating are best seen when $\Gamma_{s,g} \approx \Gamma_{a,g}$ and $\Gamma_{g,g} \approx \Gamma_{a,a} \approx \Gamma_{a,s}$. Then,

$$I(t) \propto |\rho_{a,g}(t)|^2 \propto \frac{2e^{-2\Gamma_{a,g}\tau_{12}-2\Gamma_{g,g}\tau_{2'1}-2\Gamma_{a,g}(t-\tau_{2'})}}{\omega_{s,a}^{\ 2}} \times$$
$$\{\kappa_{a,g;s,g}^{\ 2}[1-\cos(\omega_{a,s}\tau_{12})] + \kappa_{a,s;a,a}^{\ 2}[1-\cos(\omega_{a,s}\tau_{2'1})] +$$
$$\kappa_{a,g;s,g}\kappa_{a,s;a,a}[1-\cos(\omega_{a,s}\tau_{12}) - \cos(\omega_{a,s}\tau_{2'1}) +$$
$$\cos(\omega_{a,s}\tau_{12} + \omega_{a,s}\tau_{2'1})]\} \quad (4)$$

Equation 4 demonstrates that both temporal dimensions τ_{12} and $\tau_{2'1}$ beat at the $\omega_{a,s}$ frequency expected for transfers after the first and second coherences. The quantum beating in $\tau_{2'1}$ arises from amplitude-level interference of the (a, s) coherence with the (g, g) and (a, a) populations, but the beating in τ_{12} arises from interference of the (a, g) and (s, g) coherences. Time ordering IV is equivalent to time ordering III with the subscripts 2 and 2′ interchanged. The temporal dependence of time ordering I/II can be derived using a similar method.

Figure 3b is a theoretical simulation of the experimental data in Figure 3a using the approach described above (without any approximations of the dephasing rates) for time orderings I/II and III/IV. The agreement between simulation and experiment indicates that this simplified model reproduces the important features of coherence transfer. Quantum beating in the experimental data has maxima along the axes at $\tau_{2'1} = 0$ ps or $\tau_{21} =$ 0 ps, but the simulation has minima along these axes. These differences are not believed to be significant. Additionally, there are no resonant pathways in time ordering V/VI for this peak, and any intensity in these regions is generated by the finite pulse width.

Previous work in $Rh(CO)_2acac$ attributed CT peaks to a mechanism requiring two coherence transfers.[4] Although the previous results could have been explained with one transfer, two transfers were preferred because the transition dipole moments of the asymmetric and symmetric stretches are approximately orthogonal and pathways with one transfer should not be observable. In spite of this observation, Figures 2 and 3 clearly show pathways requiring one coherence transfer. Additionally, Figure 2 lacks any spectral features from pathways with two coherence transfers. Frequency-domain FWM allows unambiguous assignment of the coherence transfer mechanism by resolving pathways involving one and two transfers.

Coherence transfer offers an alternative method for examining coupled quantum states in coherent multidimensional spectroscopy. The state specificity of frequency-domain FWM and the discrimination of the $\vec{k}_{CT} = -\vec{k}_1 + \vec{k}_2 + \vec{k}_{2'}$ phase-matching condition isolate the coherence transfer pathways and enable direct experiments involving coherence transfer processes in more complex systems.

Acknowledgment. This work was supported by the National Science Foundation under grant CHE-0130947. Acknowledgment is also made to the donors of the Petroleum Research Fund of the American Chemical Society for their support of this research. This work was supported in part by a fellowship from Merck Research Laboratories.

References and Notes

(1) Wright, J. C.; Zhao, W.; Murdoch, K. M.; Besemann, D. M.; Condon, N. J.; Meyer, K. A. Nonlinear 2D Vibrational Spectroscopy. In *Handbook of Vibrational Spectroscopy*; Chambers, J. M., Griffiths, P. R., Eds.; John Wiley and Sons: New York, 2001.
(2) Mukamel, S. *Annu. Rev. Phys. Chem.* **2000**, *51*, 691.
(3) Jonas, D. M. *Annu. Rev. Phys. Chem.* **2003**, *54*, 425.
(4) Khalil, M.; Demirdoven, N.; Tokmakoff, A. *J. Chem. Phys.* **2004**, *121*, 362.
(5) Ding, F.; Fulmer, E. C.; Zanni, M. T. *J. Chem. Phys.* **2005**, *123*, 094502.
(6) Asplund, M. C.; Zanni, M. T.; Hochstrasser, R. M. *Proc. Natl. Acad. Sci. U.S.A.* **2000**, *97*, 8219.
(7) Merchant, K. A.; Thompson, D. E.; Fayer, M. D. *Phys. Rev. Lett.* **2001**, *86*, 3899.
(8) Khalil, M.; Demirdoven, N.; Tokmakoff, A. *J. Phys. Chem. A* **2003**, *107*, 5258.
(9) Pakoulev, A. V.; Rickard, M. A.; Meyer, K. A.; Kornau, K.; Mathew, N. A.; Thompson, D. E.; Wright, J. C. *J. Phys. Chem. A* **2006**, *110*, 3352.
(10) Meyer, K. A.; Wright, J. C.; Thompson, D. E. *J. Phys. Chem. A* **2004**, *108*, 11485.
(11) Besemann, D. M.; Meyer, K. A.; Wright, J. C. *J. Phys. Chem. B* **2004**, *108*, 10493.
(12) Meyer, K. A.; Besemann, D. M.; Wright, J. C. *Chem. Phys. Lett.* **2003**, *381*, 642.
(13) Rickard, M. A.; Pakoulev, A. V.; Kornau, K.; Mathew, N. A.; Wright, J. C. *J. Phys. Chem. A* **2006**, *110*, 11384.
(14) Stenholm, S. *J. Phys. B: At. Mol. Opt. Phys.* **1977**, *10*, 761.